Compass Gait Revisited: A Human Data Perspective with Extensions to Three Dimensions

Ryan W. Sinnet, Matthew J. Powell, Shu Jiang and Aaron D. Ames

Abstract— To better understand human walking, three bipedal robotic models—starting with the compass gait biped and increasing in complexity to a 3D kneed biped—are studied with controllers of human-inspired design; these controllers are derived from experimental data measuring the kinematics of human test subjects. The collected data are examined in an attempt to classify some of the most fundamental behaviors underlying human walking; it is found that a subset of functions on the kinematics of humans can be represented as a single class of functions. The control scheme uses feedback linearization to track the human output functions on a robot. A state-based parameterization for time is introduced to make these human functions time-invariant. Simulation results indicate the existence of locally exponentially stable periodic orbits for each model of interest; these orbits represent stable, steady-state walking gaits. The application of the human-inspired control approach results in "humanlike" walking as supported by agreement between the outputs of the robot models and humans.

I. INTRODUCTION

Essential to the advancement of anthropomorphic robotics is the development of control techniques which result in humanlike bipedal walking. Until recently, research in the field of robotic walking has focused on obtaining walking via mechanism design and strict control theory using passivity-based control [1], [2], control of zero-moment point [3], [4], hybrid zero dynamics [5], [6], [7], central pattern generators [8], [9], and compliance-based control [10], to name a few methods. The biomechanical component of robotic walking has been largely overlooked, though it is starting to be considered [11]. The authors' previous work [12] takes this into consideration, developing a walking controller based on experimental human walking data. Simple functions are used to model fundamental kinematics behaviors associated with human walking; these functions are tracked through feedback linearization and ultimately lead to stable, humanlike walking on an anthropomorphic model in simulation. The goal of this paper is to understand this method in the context of well-studied bipedal models with the hopes that the intuition gained will lead to improvements in the control approach.

This study of bipedal walking begins by introducing the notion of a hybrid system—a particular type of system which exhibits continuous dynamics, i.e., the dynamic model governing continuous motion, and discrete dynamics, resulting from rigid-body impacts such as foot-strike. This definition

provides a theoretical framework upon which to construct hybrid models and controllers for the models studied in this paper. After model construction, a control strategy is introduced which can be used to achieve humanlike walking on the constructed hybrid models. Specifically, human walking data are analyzed and it is found that many of the kinematics behaviors associated with human walking can be modeled using a single *canonical human function*; this concept is leveraged to construct functions encoding human walking.

Obtaining the canonical human function from experimental human data is a major result of the paper; this function gives an effective and viable representation of specific kinematic outputs of human walking, without requiring any knowledge of the intricacies of the dynamics or control governing these outputs. Indeed, the human control system responsible for walking is highly complex. From the regulation of muscle behavior via transmission of electrochemical waves in the nervous system to the generation of forces by the firing of muscle fibers, the relationship between inputs and outputs in the human motor control system can be quite challenging to decipher. We claim, however, that the most relevant outputs of the human walking control system are governed by the canonical human function (10). We can use this idea, without knowledge of the human controller or internal dynamics, to provide a control method for a robot by which we can regulate the internal dynamics, and achieve the same outputs as a human. While this discovery allows us to obtain bipedal robotic walking which is kinematically similar to human walking in simulation, the implications of this result extend far beyond simulation alone. In fact, the universality of these kinematics outputs provides insight into human walking. This result suggests that at the most basic, *innate* level, the primary outputs of the human locomotive system actually constitute a system of *spring dampers*.

Using the the canonical equation (10) and feedback linearization [13], walking is achieved on three well-studied bipedal models. Specifically, the compass gait biped [14], [15], [16], the 2D kneed biped [17], [18], and the 3D kneed biped [19] are studied. Simulations are given which show stable walking, and it is found that the results of these simulations match the human data remarkably well—an indication that the robotic walking achieved in these three models is indeed humanlike.

II. HYBRID SYSTEMS AND ROBOTIC MODELS

Hybrid systems are systems that display both continuous and discrete behavior and so bipedal walkers are naturally

Department of Mechanical Engineering, Texas A&M University, College Station, TX 77843, e-mail: {rsinnet,mjpowell,shujiang,aames}@tamu.edu

modeled by systems of this form. This section, therefore, introduces the basic terminology of hybrid systems.

A. Formal Definition of Hybrid Systems

Hybrid systems or *systems with impulse effects* [20] have been studied extensively in a wide variety of contexts and have been used to model a wide range of bipedal robotic systems [21]. In this section, we introduce a definition of hybrid systems applicable to bipedal walking.

Definition 1: A *hybrid control system* is a tuple,

$$\mathscr{HC} = (\mathcal{D}, U, S, \Delta, f, g),$$

where

- $\mathcal{D}$ is the *domain* with $\mathcal{D} \subseteq \mathcal{X}$ a smooth submanifold of the state space $\mathcal{X} \subseteq \mathbb{R}^{2n}$,
- $U \subseteq \mathbb{R}^m$ is the admissible control,
- $S \subset \mathcal{D}$ is a proper subset of $\mathcal{D}$ called the *guard* or *switching surface*,
- $\Delta : S \to \mathcal{D}$ is a smooth map called the *reset map*,
- (f, g) is a *control system* on $\mathcal{D}$, i.e., $\dot{x} = f(x) + g(x)u$.

A *hybrid system* is a hybrid control system with $U = \emptyset$, e.g., any applicable feedback controllers have been applied, making the system closed-loop. In this case,

$$\mathscr{H} = (\mathcal{D}, S, \Delta, f),$$

where f is a *dynamical system* on $\mathcal{D} \subseteq \mathcal{X}$, i.e., $\dot{x} = f(x)$.

Hybrid Period Orbits and the Poincaré Map. In order to establish the stability of k-periodic orbits, we will use the standard technique of studying the corresponding Poincaré map. In particular, taking G to be the Poincaré section, one obtains the Poincaré map, $P : G \to G$, which is a partial map defined by:

$$P(z) = c(\tau(z)).$$

where $c(t)$ is the solution to $\dot{x} = f(x)$ with $c(0) = R(z)$ and $\tau(z)$ is the *time-to-impact* function. In particular, if z^* is a k-fixed point of P (under suitable assumptions on z^*, G, and the transversality of $\mathcal{O}$ and G) a k-periodic orbit $\mathcal{O}$ with $z^* \in \mathcal{O}$ is locally exponentially stable if and only if P^k is locally exponentially stable (as a discrete-time dynamical system, $z_{i+1} = P(z_i)$). Although it is not possible to explicitly compute the Poincaré map, one can compute a numerical approximation of this map through simulation and thereby test its stability numerically. This gives a concrete method for practically testing the stability of periodic orbits.

B. Constructing Hybrid Systems

We will now show how to construct a hybrid system for a biped given a Lagrangian and a discrete event (in this case, foot strike). We begin with the assumption that the stance foot is pinned to the ground and use this to describe the continuous dynamics. In order to derive the discrete dynamics, we must introduce additional Cartesian coordinates ψ, w_x, w_y, w_z at the stance foot with ψ a rotation about the z-axis. A more general discussion applicable to a wider range of bipeds can be found in [21].

Domain and Guard. The domain specifies the allowable configuration of the system. For the models considered in this paper, the non-stance foot must be above the ground. This condition is specified by a unilateral constraint, h, which naturally leads to a definition for the domain:

$$\mathcal{D} = \{(q, \dot{q}) \in T\mathcal{Q} : h(q) \geq 0\}. \tag{1}$$

The guard is just the boundary of the domain with the additional assumption that the unilateral constraint is decreasing, i.e., the vector field is pointed outside of the domain, or

$$S = \left\{(q, \dot{q}) \in T\mathcal{Q} : h(q) = 0 \text{ and } \frac{\partial h(q)}{\partial q}\dot{q} < 0\right\}. \tag{2}$$

Continuous Dynamics. The Lagrangian of a bipedal robot, $\mathcal{L} : T\mathcal{Q} \to \mathbb{R}$, can be stated in terms of the kinetic energy, $K : T\mathcal{Q} \to \mathbb{R}$, and the potential energy, $V : \mathcal{Q} \to \mathbb{R}$, as $\mathcal{L}(q, \dot{q}) = K(q, \dot{q}) - V(q)$. The Euler-Lagrange equation gives the dynamic model, which, for robotic systems (see [22]), is stated as:

$$D(q)\ddot{q} + H(q, \dot{q}) = B(q)u \tag{3}$$

with inertia map $D(q)$ and torque distribution map $B(q)$, and

$$H(q, \dot{q}) = C(q, \dot{q})\dot{q} + G(q)$$

containing terms resulting from the Coriolis effect and gravity; $C(q, \dot{q})$ can be found using standard methods [22]. Manipulation of (3) leads to the control system (f, g):

$$f(q, \dot{q}) = \begin{bmatrix} \dot{q} \\ -D^{-1}(q)H(q, \dot{q}) \end{bmatrix}, \quad g(q) = \begin{bmatrix} \mathbf{0} \\ D^{-1}(q)B(q) \end{bmatrix}. \tag{4}$$

Discrete Dynamics. In order to define the reset map, it is necessary to first augment the configuration space $\mathcal{Q}$. Attach a frame R_e to the stance foot; then w represents the Cartesian position of R_e and $\psi \in \mathbb{S} \subset SO(3)$[1] represents the orientation of R_e about the z-axis. The *generalized coordinates* are then written

$$q_e = (p_x, p_y, p_z, \psi, q) \in \mathcal{Q}_e = \mathbb{R}^3 \times \mathbb{S} \times \mathcal{Q}.$$

Without loss of generality, we assume that the values of the extended coordinates are zero throughout the gait. Moreover, the configuration variable does not change through impact so these values will be zero right after impact. Therefore, we introduce the embedding $\iota : \mathcal{Q} \to \mathcal{Q}_e$ defined by $(0, 0, 0, 0, q) \mapsto q_e$; this will allow us to write the generalized coordinates in terms of the shape coordinates.[2]

The impact model [23] under consideration assumes that an impulsive force is applied at the non-stance foot upon impact. This motivates the use of the holonomic constraint

$$J(q)\dot{q} = \begin{bmatrix} v \\ \omega_z \end{bmatrix},$$

---

[1] $SO(n)$ represents the special orthogonal group in n dimensions.
[2] For a biped in two dimensions (in the xz-plane), it is only necessary to consider the additional coordinates p_x and p_z.

(a) CG model   (b) K2 model   (c) K3 model

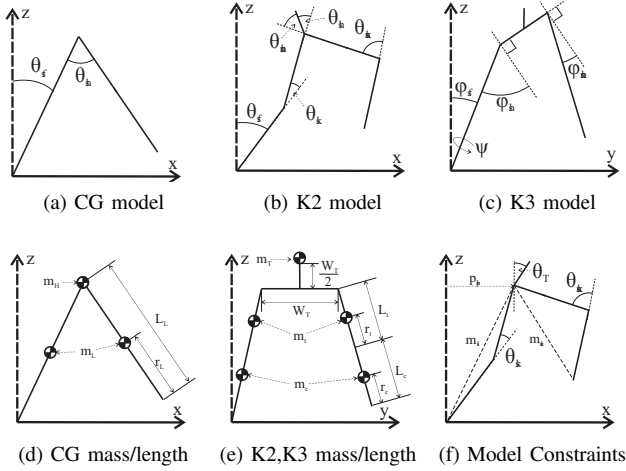(d) CG mass/length   (e) K2,K3 mass/length   (f) Model Constraints

Fig. 1: Configuration, and the mass and length distribution, for compass gait (CG), 2D kneed (K2), and 3D kneed (K3) models. Values for parameters are available online [26].

with $J(q)$ a Jacobian matrix, $v = \dot{w}$ the velocity of R_e, and ω_z the angular velocity of R_e about the body-fixed z-axis.[3] An impulsive wrench is used to impose these constraints through impact. Specifically, the configuration q does not change through impact and the post-impact velocity $\dot{q}^+$ is given in terms of the pre-impact velocity $\dot{q}^-$ by balancing angular momentum. Using the Schur complement (see [25]), the post-impact velocity can be written as a map:

$$\dot{q}^+ = P(q_e, \dot{q}_e^-) = \qquad\qquad\qquad (5)$$
$$(I - D^{-1}(q_e)J^T(q_e)(J(q_e)D^{-1}(q_e)J(q_e))^{-1}J(q_e))\dot{q}_e^-$$

with I the identity matrix.

Motivated by the desire to simplify a bipedal model and obtain biperiodic behavior, the left and right legs must be "swapped" at impact; this trick is common throughout the literature [20]. A coordinate transformation $\mathcal{R}$ (i.e., a *state relabeling procedure*) switches the roles of the left and right legs and is included in the reset map:

$$\Delta(q, \dot{q}) = \begin{bmatrix} \mathcal{R} & \mathbf{0} \\ \mathbf{0} & \mathcal{R} \end{bmatrix} \begin{bmatrix} \pi \circ \iota(q) \\ \pi^* \circ P(\iota(q), \iota^*(\dot{q})) \end{bmatrix}, \quad (6)$$

where ι^* is the pushforward of ι and π is the canonical projection associated with ι with pushforward π^*. The reset map (6) takes a point on the guard and maps it to the domain.

C. BIPEDAL MODELS

Three related point-foot bipedal models will be considered in this paper; these models are shown in Fig. 1. In order of increasing complexity, these models are: 2D compass-gait (CG) biped, 2D kneed biped (K2), 3D kneed biped (K3). We will now describe the construction of these models.

2D Compass Gait Biped (CG). The 2D compass gait biped consists of two links with physical parameters given

[3]The body-fixed angular velocity ω_z can be found using standard kinematics analysis methods [24].

in Fig. 1(d). For this model, the configuration space $\mathcal{Q}_{\mathrm{CG}}$ has coordinates

$$q_{\mathrm{CG}} = (\theta_{sf}, \theta_{sh})^T.$$

Combining these coordinates with the configuration of the model as given in Fig. 1(a) results in Lagrangian $\mathcal{L}_{\mathrm{CG}}(q_{\mathrm{CG}}, \dot{q}_{\mathrm{CG}})$. Assuming full control authority, i.e., $U_{\mathrm{CG}} = \mathbb{R}^2$, one obtains the appropriate control system $(f_{\mathrm{CG}}, g_{\mathrm{CG}})$ as is given by (4).

Let $h_{\mathrm{CG}}(q_{\mathrm{CG}})$ be a unilateral constraint representing the height of the non-stance foot above the ground. Using the methods of Sec. II leads to the domain $\mathcal{D}_{\mathrm{CG}}$ and guard S_{CG} given by (1) and (2), respectively.

The reset map Δ_{CG} is given by (6); the corresponding relabeling map $\mathcal{R}_{\mathrm{CG}}$ is given by

$$(\theta_{sf} + \theta_{sh}, -\theta_{sh}) \longmapsto (\theta_{sf}, \theta_{sh}).$$

We can now express the hybrid control system for the model CG as

$$\mathscr{HC}_{\mathrm{CG}} = (\mathcal{D}_{\mathrm{CG}}, U_{\mathrm{CG}}, S_{\mathrm{CG}}, \Delta_{\mathrm{CG}}, f_{\mathrm{CG}}, g_{\mathrm{CG}}). \quad (7)$$

2D Kneed Biped (K2). The 2D kneed biped has knees and a torso for a total of five links with physical parameters given in Fig. 1(e). The configuration space $\mathcal{Q}_{\mathrm{K2}}$ has coordinates

$$q_{\mathrm{K2}} = (\theta_{sf}, \theta_{sk}, \theta_{sh}, \theta_{nsh}, \theta_{nsk})^T.$$

Combining these coordinates with the configuration of the model as given in Fig. 1(b) results in Lagrangian $\mathcal{L}_{\mathrm{K2}}(q_{\mathrm{K2}}, \dot{q}_{\mathrm{K2}})$. We again assume full control authority, i.e., $U_{\mathrm{K2}} = \mathbb{R}^5$, and obtain control system $(f_{\mathrm{K2}}, g_{\mathrm{K2}})$ as in (4).

Let $h_{\mathrm{K2}}(q_{\mathrm{K2}})$ be a unilateral constraint representing the height of the non-stance foot above the ground; this constraint naturally leads to domain $\mathcal{D}_{\mathrm{K2}}$ and guard S_{K2} given by (1) and (2), respectively.

The reset map Δ_{K2} is given by (6) with relabeling map $\mathcal{R}_{\mathrm{K2}}$ given by

$$(-\theta_{sf} - \theta_{sk} - \theta_{sh} + \theta_{nsh} + \theta_{nsk}, \theta_{nsk}, \theta_{nsh}, \theta_{sh}, \theta_{sk})$$
$$\longmapsto (\theta_{sf}, \theta_{sk}, \theta_{sh}, \theta_{nsh}, \theta_{nsk}).$$

We can now express the hybrid control system for the model K2 as

$$\mathscr{HC}_{\mathrm{K2}} = (\mathcal{D}_{\mathrm{K2}}, U_{\mathrm{K2}}, S_{\mathrm{K2}}, \Delta_{\mathrm{K2}}, f_{\mathrm{K2}}, g_{\mathrm{K2}}). \quad (8)$$

3D Kneed Biped (K3). The 3D kneed biped has knees and a hip with two degrees of freedom at each hip joint. Like K2, this model has five links; however, this model operates in three dimensions and thus requires additional coordinates. The physical parameters are shown in Fig. 1(e) and the configuration space $\mathcal{Q}_{\mathrm{K3}}$ for K3 has coordinates

$$q_{\mathrm{K3}} = (\varphi_{sf}, \theta_{sf}, \theta_{sk}, \theta_{sh}, \varphi_{sh}, \varphi_{nsh}, \theta_{nsh}, \theta_{nsk})^T.$$

Combining these coordinates with the configuration of the model as given in Fig. 1(c) results in a Lagrangian $\mathcal{L}_{\mathrm{K3}}$. Assuming full control authority, i.e., $U_{\mathrm{K3}} = \mathbb{R}^8$, one obtains the appropriate control system $(f_{\mathrm{K3}}, g_{\mathrm{K3}})$ as is given by (4).

Let $h_{K3}(q_{K3})$ be a unilateral constraint representing the height of the non-stance foot above the ground; this constraint naturally leads to domain $\mathcal{D}_{K3}$ and guard S_{K3} given by (1) and (2), respectively.

Because K3 operates in three dimensions, the reset map is more complicated. The impact map $P_{K3} : S_{K3} \to \mathcal{D}_{K3}$ given by (5) is used with generalized coordinates as described in Sec. II. The additional complexity arises in the state relabeling procedure. The coordinates other than those at the foot are exchanged viz.

$$(\theta_{nsk}, \theta_{nsh}, \varphi_{nsh}, \varphi_{sh}, \theta_{sh}, \theta_{sk})$$
$$\longmapsto (\theta_{sk}, \theta_{sh}, \varphi_{sh}, \varphi_{nsh}, \theta_{nsh}, \theta_{nsk}).$$

The coordinates at the new stance foot, φ_{sf} and θ_{sk}, and their associated velocites are found via a nonlinear transformation as described in [27]. The reset map Δ_{K3} is given by applying the state relabeling procedure just described to the impact map $P_{K3}(q_{K3}, \dot{q}_{K3})$.

We can now express the hybrid control system for the model K3 as

$$\mathcal{HC}_{K3} = (\mathcal{D}_{K3}, U_{K3}, S_{K3}, \Delta_{K3}, f_{K3}, g_{K3}). \quad (9)$$

III. HUMAN-INSPIRED CONTROLLER DESIGN

In Sec. II, we introduced hybrid systems and showed how to construct hybrid models for the bipeds of interest in this paper. Our goal now is to develop control laws which result in stable humanlike walking when applied to the hybrid control systems $\mathcal{HC}_{CG}$, $\mathcal{HC}_{K2}$, and $\mathcal{HC}_{K3}$. Motivated by our desire to mimic human walking in some capacity, we will draw inspiration from experimental human kinematics data. Specifically, we will design functions which mimic some of the fundamental behaviors of human walking and track these human functions using feedback linearization. Before going into detail on the function design process, a description of the experiment is appropriate.

A. Experimental Setup

The Phase Space System [28] comprises 12 high precision cameras positioned to allow for spatial measurements of a number of LED sensors to within an accuracy of one millimeter. For a given test subject, we fixed 19 LED sensors at strategic points on the subject and instructed the subject to walk straightly on flat ground. We collected the positions of the sensors at 480 Hz. We repeated the process 11 times for a given subject—three of the test runs represent normal walking while the other eight represent fast walking, slow walking, backward walking, etc. Overall, we measured the gait of nine subjects; the collected data are available online [29]. In this paper, we selected the subject whose data were the least noisy—we use these data for the controller design process specified presently.

B. Extracting Human Functions from Data

We now describe the process of designing human functions which characterize behaviors fundamental to human walking. From this point on, it is assumed that we are considering the
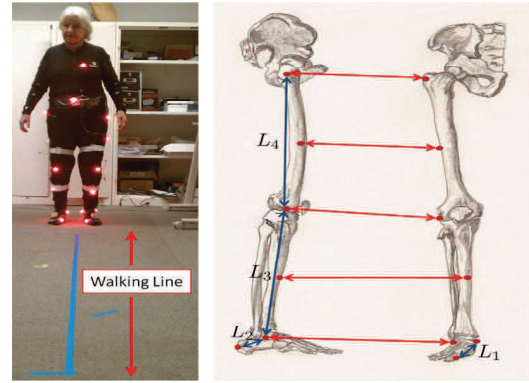

Fig. 2: The experimental setup. Left—placement of the sensors on test subject; the walking path is in blue. Right—leg sensor locations.

data for a single test subject; specifically, we consider subject four for the rest of this paper.

Canonical Human Function. Using the data for our chosen subject, we examine various output functions on the subject's kinematics, i.e., we consider angles, slopes, and end-effector positions. The idea is to determine a set of behaviors which can be used to represent human walking.[4] We found that the following functions (see Fig. 1(f)) describe fundamental behaviors intrinsic to human walking: sagittal leg slopes, knee angles, torso angle and hip velocity. In the coronal plane, we examined the angles of the hip and the angle between the stance leg and the ground.

One of the primary motivations behind this choice of functions is the trajectory each function follows over time. Each of behaviors mentioned qualitatively resembles a second-order system response and can thus be characterized with the following canonical human function:

$$y^d(t) = \quad (10)$$
$$e^{-a_5 t}(a_1 \cos(a_2 t + a_3) + a_4 \sin(a_2 t + a_3)) + a_6 t + a_7.$$

Function Fitting. We would like to apply the cannonical human function (10) to our data to model the behaviors described. Formally, this means that we would like to find the parameters $a_1, \ldots, a_7$ for a given function which result in functions that fit the data closely as possible; in other words, for each function, we would like to solve the optimization problem

$$\min_{\{a_i\}_{i=1}^7} \sum_{k=1}^{K} (y_d(\tau[k], a_i, \ldots, a_7) - x[k])^2, \quad (11)$$

where $\tau[k]$ and $x[k]$ represent the time and human data, respectively, with $k \in [1, \ldots, K] \subset \mathbb{Z}$ an index for the K data points, and $y_d(\cdot)$ the fitting function with parameters

[4]When deciding on a choice of functions, it is necessary to choose one function for each degree of actuation. Moreover, a good choice of functions is one in which there is an approximate one-to-one correspondance between actuators and functions. For example, we would not want to track both the angle and slope of the stance leg as one actuator would do most of the work in tracking these functions.

$a_1, \ldots, a_7$. To be clear, $x[k]$ is the value of the kinematics function on the human at data point k.

Solving the optimization problem (11) parameters for the chosen functions; these parameters are given in Table I. The correlations, as given in the same table, show that the fitted functions very closely model the human data. Indeed, the coefficients of correlation are all between 0.984 and 0.999. The accuracy can best be seen in Fig. 4. It is important to note that we also track the angle of the torso in two of our three models (K2 and K3); however, the magnitude of motion is relatively small and thus has comparatively little effect on the dynamics of the system. We therefore decide to track the mean value of the torso angle for the sake of simplicity.

C. Function Tracking through Feedback Linearization

The human functions described by (10) with parameters given in Table I essentially encode the human gait. In order to reproduce this gait on the robotic models under consideration, a control strategy must be leveraged to track these functions. The particular control method we will use is feedback linearization (see [13, ch. 9]). As a general goal, we would like to achieve autonomous (time-invariant) feedback. Yet the canonical human function (10) is time-dependent. To this end, we will first describe a control law which achieves walking with time-dependent functions; then, we will introduce a state-based parameterization in order to express (10) as a state-dependent function without time dependence. Then, we will describe a control law which achieves walking using this autonomous function.

Time-Based (TB) Feedback Control. As mentioned, we will use feedback linearization to track (10). To begin, define the virtual output

$$y(q, t) = y_a(q) - y_d(t). \tag{12}$$

To satisfy the ouputs (15), we use the standard method of feedback linearization (see [13, ch. 9]., Because we are tracking functions of position q which have no dependence on velocitiy $\dot{q}$, we have a relative degree two system. Our goal is to drive (12) to zero, i.e., $y(q, \dot{q}, t) \to 0$. Using the Lie derivative notation $L_{f(x)}y(x) = \frac{dy}{dx}f(x)$ for $\dot{x} = f(x)$, the control law which accomplishes this is given by

$$u^{\text{TB}}(q, \dot{q}, t) = -(L_g L_f y_2(q, t))^{-1} \cdot \tag{13}$$
$$\left(L_f L_f y(q, t) + 2\varepsilon L_f y(q, t) + \varepsilon^2 y(q, t)\right)$$

with control gain ε for control system (f, g). Applying this control law yields

$$f_{cl}(q, \dot{q}) = f(q, \dot{q}) + g(q) \, u^{\text{TB}}(q, \dot{q}, t).$$

Time-Invariant Parameterization. Motivated by our desire to design *autonomous* or *time-invariant* controllers, we introduce a parameterization for time as is common in the literature [5], [7].

Denote the parameterization by $\varsigma : Q \to \mathbb{R}_0^+$ where $\mathbb{R}_0^+$ represents forward time;

Fig. 3: Forward position of hip.

we would like $\varsigma(t)$ to be approximately linear, i.e., $\varsigma(t) \approx \alpha t$ for some α. From Fig. 3, we see that $p_{hip}^x \approx \bar{v}_{hip}^x t$ with $\bar{v}_{hip}^x$ the average x velocity of the hip; this approximately linear relationship motivates the following parameterization:

$$\varsigma(t) := \frac{p_{hip}^x(q) - p_{hip}^x(q^-)}{\bar{v}_{hip}^x}. \tag{14}$$

We choose to track v_{hip}^x, driving it to a constant. The value of this constant should be the parameter $\bar{v}_{hip}^x$ from (14).

Autonomous (AT) Feedback Control. The parameterization (14) is a map from state to time and is applied to the desired human functions. Motivated by our desire to track the human functions and using (14), we define the following virtual output:

$$y(q, \dot{q}) = y^a(q, \dot{q}) - y^d(\varsigma(q))$$

with y^a the actual function on the kinematics of the robot and y^d the desired value from the human functions. Because of the use of hip velocity, we have a mixed relative degree system. Group the output functions as

$$y(q, \dot{q}) = (y_1^T(q, \dot{q}), y_2^T(q))^T, \tag{15}$$

where y_1 and y_2 represent the relative degree one and two outputs respectively. Similar to the time-based case, the
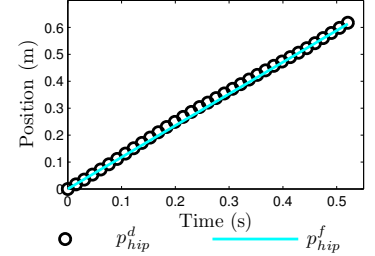
TABLE I: Optimized parameter values for human functions.

$y^d = \frac{a_1 \cos(a_2 t + a_3) + a_4 \sin(a_2 t + a_3)}{e^{a_5 t}} + a_6 t + a_7$								
f.	a_1	a_2	a_3	a_4	a_5	a_6	a_7	Corr.
m_{sl}	0	0	0	0	0	-1.267	0.249	0.995
m_{nsl}	0	7.46	-2.452	-0.404	0	0	-0.119	0.999
θ_{sk}	-0.082	13.31	0	0.207	4.154	0	0.257	0.99
θ_{nsk}	-0.380	10.979	0	0.197	-0.421	0	0.658	0.993
φ_{sh}	-0.028	14.480	0.830	0.008	1.166	0	.206	0.990
φ_{nsh}	0	13.209	-4.161	0.053	0	0	0.158	0.992
φ_{sa}	0	0	0	0	0	-0.259	-0.184	0.984
p_{hip}^x	0	0	0	0	0	1.177	0.705	0.999
θ_T	0	0	0	0	0	0	0.059	0

TABLE II: Function choices for models of interest.

Function	CG (TB)	CG (AT)	K2 (TB)	K2 (AT)	K3 (TB)
m_{sl}	●		●		●
m_{nsl}	●	●	●	●	●
θ_{sk}			●	●	●
θ_{nsk}			●	●	●
θ_T			●	●	●
v_{hip}^x		●		●	
φ_{sh}					●
φ_{nsh}					●
φ_{sf}					●

(a) Slope constraints   (b) Sagittal Angular Constraints   (c) Coronal Angular Constraints
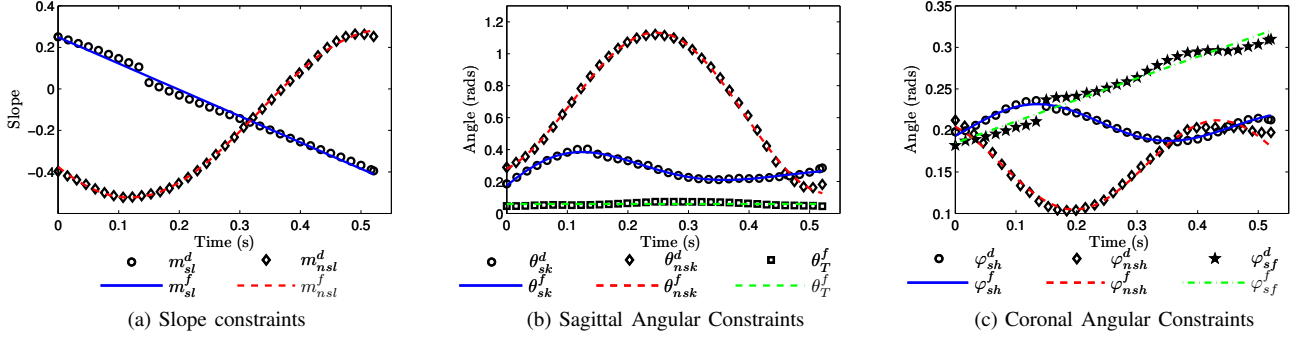
Fig. 4: Human data over the course of one step with one leg and the "canonical" functions that are fitted to this data. The specific variables that are plotted can be seen in Table I.
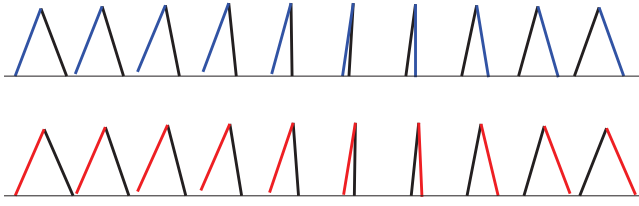

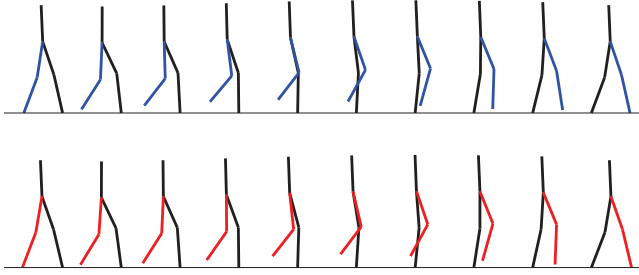Fig. 5: Walking with TB (top)/AT (bottom) on model CG.

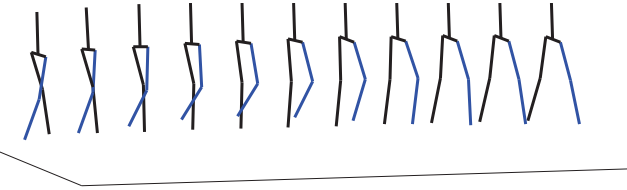Fig. 6: Walking with TB (top)/AT (bottom) on model K2.

Fig. 7: Walking with TB on model K3.

control law which drives $y(q, \dot{q}) \to 0$ is given by

$$u^{\text{AT}}(q, \dot{q}) = -\mathcal{A}^{-1}(q, \dot{q}) \left(\begin{bmatrix} 0 \\ L_f L_f y_2(q) \end{bmatrix} \right. \tag{16}$$
$$\left. + \begin{bmatrix} L_f y_1(q, \dot{q}) \\ 2\varepsilon L_f y_2(q, \dot{q}) \end{bmatrix} + \begin{bmatrix} \varepsilon y_1(q, \dot{q}) \\ \varepsilon^2 y_2(q) \end{bmatrix} \right),$$

with control gain ε and decoupling matrix $A(q)$ given by

$$\mathcal{A}(q, \dot{q}) = \begin{bmatrix} L_g y_1(q, \dot{q}) \\ L_g L_f y_2(q, \dot{q}) \end{bmatrix}$$

for a given control system (f, g). We apply this control law:

$$f_{cl} = f(q, \dot{q}) + g(q) u^{\text{AT}}(q, \dot{q}).$$
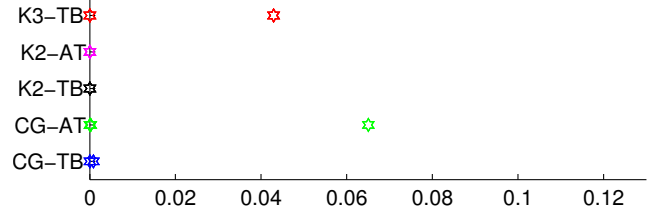

Fig. 8: Eigenvalue magnitudes for all models.

IV. SIMULATION RESULTS

In this section, we describe simulations modeling the bipeds discussed. For models CG and K2, we simulate both TB and AT control, and for model K3 we simulate only TB. Through trial and error, we found that tracking the stance leg slope with TB control is the best choice; however, we achieve better results with AT control by replacing the stance leg slope with the velocity of the hip.

Hybrid System Construction. In order conduct a given simulation, we must construct a closed-loop hybrid system by applying some form of feedback control to a hybrid control system. We do this for each of the models: we apply (13) to (7), (8), (9) to obtain the hybrid systems $\mathscr{H}_{\text{CG}}^{\text{TB}}$, $\mathscr{H}_{\text{K2}}^{\text{TB}}$, $\mathscr{H}_{\text{K3}}^{\text{TB}}$, respectively; we apply (16) to (7) and (8) to obtain $\mathscr{H}_{\text{CG}}^{\text{AT}}$ and $\mathscr{H}_{\text{K2}}^{\text{AT}}$, respectively. The control gains for the CG models are set to $\varepsilon = 15$ and the gains for the K2 and K3 models are set to $\varepsilon = 50$. The human functions used in the control laws (13) and (16) are given in Table II.

Stability Analysis. Fixed points were found for each model—the presence of a fixed point implies the existence of a periodic orbit. The eigenvalues (see Fig. 8) are all below unity implying that the respective periodic orbits are locally exponentially stable.

A. Compass Gait (CG) Simulation Results

The phase portraits for the TB and AT CG models are shown in Fig. 9(a); the behaviors agree with the human data. This trend is further confirmed in the plots of the virtual outputs, Figs. 9(b) and 9(c). It is important to note that, in order to achieve walking in the CG models, we had to shift the y-intercept of the m_{nsl}^d output function from -0.119 to 0; this allowed the non-stance leg to clear the ground. This is the

only parameter we had to alter, and we used this parameter change in the K2 and K3 models to maintain consistency.

B. 2D Kneed Biped (K2) Simulation Results

The phase portraits for the TB and AT K2 models are shown in Figs. 9(d) and 9(e). Examination of these figures reveals that AT control and TB control result in slightly different behaviors. This discrepancy is even more pronounced in Figs. 9(f), 9(g), 9(h), 9(i). The difference in the behaviors of the two K2 models is a result of the parameterization of time, ς (14), which we use to obtain state feedback control; ς is linear in time with respect to the human data, however, it becomes slightly nonlinear when used as a parameterization of time in the autonomous model. The nonlinearity in ς has a greater effect on the system as the complexity of the bipedal robotic model increases; thus, the discrepancy in behaviors is more apparent in the K2 models than in the CG models.

C. 3D Kneed Biped (K3) Simulation Results

The phase portraits for the TB model are shown in Figs. 9(j), 9(k), 9(l). The phase portraits show the inherent biperiodicity of 3D walking, as a set of two limit cycles for each angle, which is incurred by the "sway" of the hips in the lateral plane. We assume this swaying motion to be relatively insignificant to the overall walking, see [19]; as such, to obtain walking, we scale down the functions for the lateral angle constraints of the human. This scaling is shown in Fig. 9(o) along with the sagittal output constraints in Figs. 9(m) and 9(n). The slight discrepancy between the K3 and the human from tracking 2D angle projections.

V. CONCLUDING REMARKS AND FUTURE WORK

In this paper, we showed that kinematics outputs of human walking can be represented by a single mathematical function. This result allows us to construct walking controllers for bipedal robots without any knowledge of the human's complex internal dynamics or control methods. The human functions are relatively "simple" yet, when implemented via feedback linearization control, yield locally exponentially stable, periodic orbit or in other words, stable walking gaits, which are remarkably humanlike in nature.

The methods presented seem to be easily extensible: in [30], the canonical human walking function is used to achieve stable walking in the simulation of a human with a transfemoral prosthesis. In [31], a method is presented for obtaining the parameters of the canonical functions in a manner which guarantees stable walking. Our current goal is to utilize these methods to achieve walking on our 10-DOF bipedal robot, AMBER. Videos can be found online [32].

REFERENCES

[1] M. W. Spong and F. Bullo, "Controlled symmetries and passive walking," *IEEE TAC*, vol. 50, no. 7, pp. 1025–1031, 2005.

[2] S. Collins, A. Ruina, R. Tedrake, and M. Wisse, "Efficient bipedal robots based on passive-dynamic walkers," *Science*, vol. 307, pp. 1082–1085, Feb. 2005.

[3] M. Vukobratović and B. Borovac, "Zero-moment point—thirty-five years of its life," *Intl. J. of Humanoid Robotics*, vol. 1, no. 1, pp. 157–173, mar 2005.

[4] S. Kajita, F. Kanehiro, K. Kaneko, K. Fujiwara, K. Harada, K. Yokoi, and H. Hirukawa, "Biped walking pattern generator allowing auxiliary zmp control," in *IEEE/RSJ Intl. Conf. on Intelligent Robots and Systems*, Beijing, May 2006, pp. 2993–2999.

[5] E. R. Westervelt, J. W. Grizzle, and D. E. Koditschek, "Hybrid zero dynamics of planar biped walkers," *IEEE TAC*, vol. 48, no. 1, pp. 42–56, Jan. 2003.

[6] C. Chevallereau, D. Djoudi, and J. W. Grizzle, "Stable bipedal walking with foot rotation through direct regulation of the zero moment point," *IEEE TRO*, vol. 25, no. 2, pp. 390–401, Apr. 2008.

[7] E. R. Westervelt, J. W. Grizzle, C. Chevallereau, J. H. Choi, and B. Morris, *Feedback Control of Dynamic Bipedal Robot Locomotion*. Boca Raton: CRC Press, Jun. 2007.

[8] T. Reil and P. Husbands, "Evolution of central pattern generators for bipedal walking in a real-time physics environment," *IEEE Transactions on Evolutionary Computation*, vol. 6, pp. 159–168, Apr. 2002.

[9] K. Tsuchiya, S. Aoi, and K. Tsujita, "Locomotion control of a biped locomotion robot using nonlinear oscillators," in *IEEE/RSJ Intl. Conf. on Intelligent Robots and Systems*, Oct. 2003, pp. 1745–1750.

[10] J. Pratt, P. Dilworth, and G. Pratt, "Virtual model control of a bipedal walking robot," in *IEEE Conf. on Robotics and Automation*, Albuquerque, Apr. 1997, pp. 193–198.

[11] D. H. Sutherland, K. R. Kaufman, and J. R. Moitoza, *Human Walking*, 3rd ed. Baltimore: Lippincott Williams & Wilkins, 2005, ch. Kinematics of Normal Human Walking, pp. 23–44.

[12] R. W. Sinnet, M. J. Powell, R. P. Shah, and A. D. Ames, "A human-inspired hybrid control approach to bipedal robotic walking," in *18th IFAC World Congress*, Milano, Aug. 2011.

[13] S. S. Sastry, *Nonlinear Systems: Analysis, Stability and Control*. New York: Springer, 1999.

[14] T. McGeer, "Passive dynamic walking," *Intl. J. of Robotics Research*, vol. 9, no. 2, pp. 62–82, Apr. 1990.

[15] B. Espiau and A. Goswami, "Compass gait revisited," in *IFAC Symposium on Robot Control*, Capri, Sep. 1994, pp. 839–846.

[16] A. Goswami, B. Thuilot, and B. Espiau, "A study of the passive gait of a compass-like biped robot: Symmetry and chaos," *IJRR*, vol. 17, no. 12, pp. 1282–1301, Dec. 1998.

[17] V. F. H. Chen, "Passive dynamic walking with knees: A point foot model," M.S. thesis, MIT, Feb. 2007.

[18] T. McGeer, "Passive walking with knees," in *IEEE Intl. Conf. on Robotics and Automation*, Cincinnati, May 1990, pp. 1640–1645.

[19] A. D. Ames, R. W. Sinnet, and E. D. B. Wendel, "Three-dimensional kneed bipedal walking: A hybrid geometric approach," in *12th ACM Intl. Conf. on Hybrid Systems: Computation and Control, Lecture Notes in Computer Science—HSCC 2009*, R. Majumdar and P. Tabuada, Eds., vol. 5469, San Francisco, Apr. 2009, pp. 16–30.

[20] J. W. Grizzle, G. Abba, and F. Plestan, "Asymptotically stable walking for biped robots: Analysis via systems with impulse effects," *IEEE TAC*, vol. 46, no. 1, pp. 51–64, Jan. 2001.

[21] J. W. Grizzle, C. Chevallereau, A. D. Ames, and R. W. Sinnet, "3D bipedal robotic walking: models, feedback control, and open problems," in *IFAC NOLCOS*, Bologna, Sep. 2010.

[22] R. M. Murray, Z. Li, and S. S. Sastry, *A Mathematical Introduction to Robotic Manipulation*. Boca Raton: CRC Press, 1994.

[23] Y. Hürmüzlü and D. B. Marghitu, "Rigid body collions of planar kinematic chains with multiple contact points," *Intl. J. of Robotics Research*, vol. 13, no. 1, pp. 82–92, Feb. 1994.

[24] R. N. Jazar, *Theory of Applied Robotics: Kinematics, Dynamics, and Control*, 1st ed. Springer, 2007.

[25] F. Zhang, *The Schur Complement and Its Applications*, ser. Numerical Methods and Algorithms Series. New York: Springer, 2005.

[26] http://www1.mengr.tamu.edu/aames/cdc_2011_spja_01/.

[27] J. W. Grizzle, C. Chevallereau, and C. Shih, "HZD-based control of a five-link underactuated 3D bipedal robot," in *IEEE Conf. on Decision and Control*, Cancún, Dec. 2008.

[28] http://www.phasespace.com/.

[29] http://www.eecs.berkeley.edu/~ramv/HybridWalker.

[30] R. W. Sinnet, H. Zhao, R. P. Shah, and A. D. Ames, "Prosthetic walking," in *IEEE/RSJ International Conference on Intelligent Robots and Systems*, San Francisco, 2011.

[31] A. D. Ames, "First steps toward automatically generating bipedal robotic walking from human data," in *8th International Workshop on Robotic Motion and Control*, Bukowy Dworek, 2011.
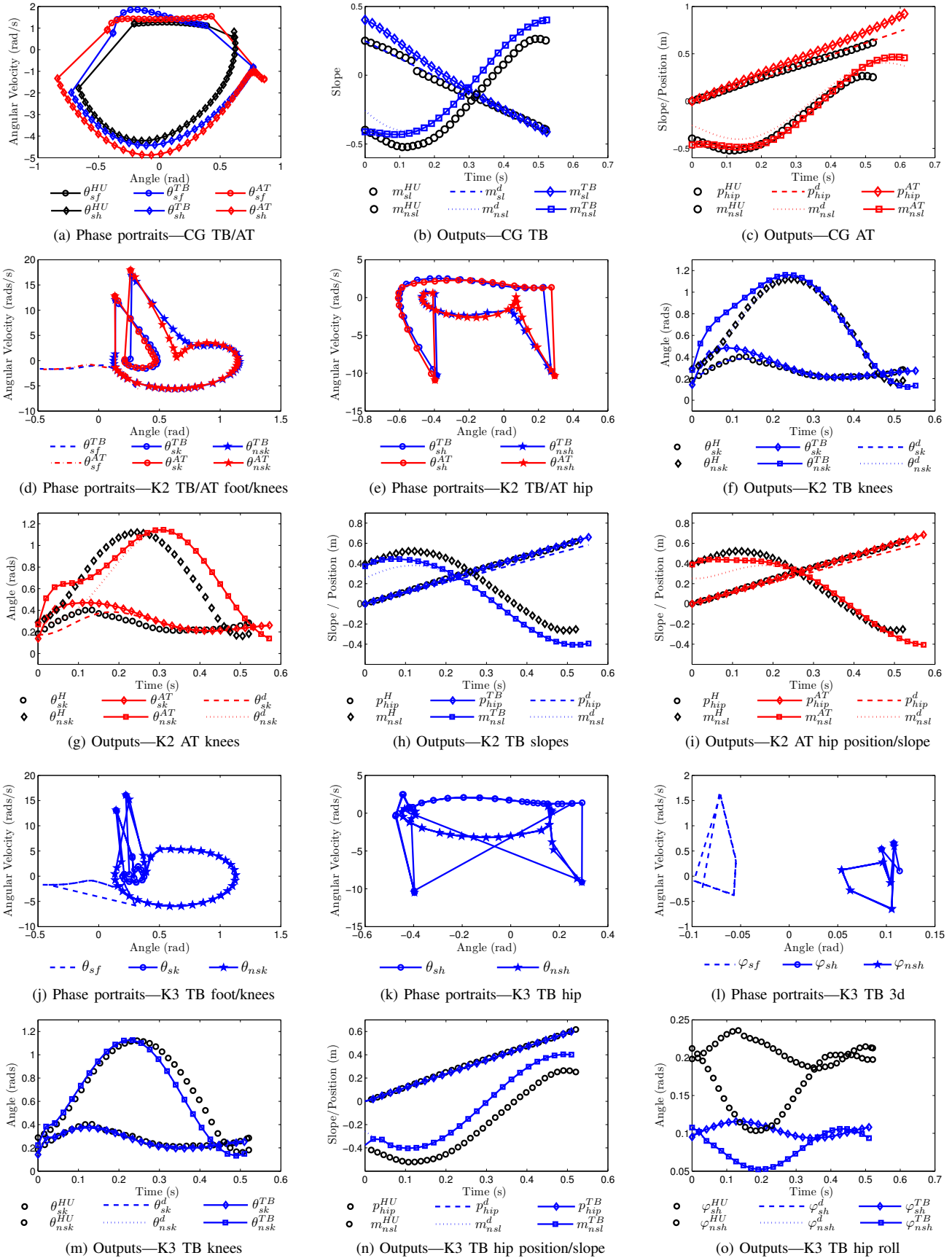
[32] http://www.bipedalrobotics.com/index.html.

Fig. 9: Phase portraits and human function tracking.